Iranian Journal of Basic Medical Sciences
ijbms.mums.ac.ir

Hyaluronic acid-coated niosomal sorafenib targets CD44 and suppresses NF-κB signalling in oral squamous cell carcinoma

Ting Wu [1], Yongshuo Li [2], Zixian Wang [3], Bin Guo [2]*

[1] Department of Stomatology, Shungeng Campus, Jinan Stomatological Hospital, No.73, Shungeng Road, Shizhong District, Jinan, Shandong, 250001, China
[2] Department of Stomatology, Central Hospital affiliated to Shandong First Medical University, No.105, Jiefang Road, Lixia District, Jinan, Shandong, 250013, China
[3] Department of Stomatology, Shandong Medical College, No 5460, Second Ring South Road, Jinan, Shandong, 250002, China

ARTICLE INFO

Article type:
Original

Article history:
Received: May 15, 2025
Accepted: Nov 10, 2025

Keywords:
Carcinoma
CD44
Drug delivery systems
Hyaluronic acid
Mouth neoplasms NF-kappa B
Sorafenib
Squamous cell

ABSTRACT

Objective(s): Oral squamous cell carcinoma (OSCC) remains highly lethal and is driven, in part, by chronic NF-κB-mediated inflammation. Sorafenib, a multikinase inhibitor of RAF/VEGFR/PDGFR, can suppress these pathways, but its clinical utility is limited by hydrophobicity, toxicity, and poor tumor penetration. We engineered hyaluronic acid-coated niosomes encapsulating sorafenib (SOR@Nio/HA) to enable CD44-targeted delivery to OSCC cells.

Materials and Methods: SOR@Nio/HA displayed a mean hydrodynamic diameter of 177±8 nm (PDI=0.23-0.26) and high encapsulation efficiency (88.3 %), with pH-responsive release (45% at pH=5.5 and 30% at pH=7.4, in 24 hr).

Results: In CAL27 cells, SOR@Nio/HA significantly enhanced cytotoxicity versus free sorafenib, lowering IC_{50} from 11.8±1.1 μM to 5.2±0.9 μM (P<0.01), and increased Annexin V/PI-defined apoptosis relative to controls. qRT-PCR showed suppression of NF-κB targets, with COX-2 and MMP-9 reduced to 0.35-fold and 0.32-fold of the control, respectively, alongside a pro-apoptotic shift in the BAX/BCL-2 axis.

Conclusion: Collectively, these data indicate that SOR@Nio/HA improves intracellular delivery and potentiates sorafenib's antitumor activity by CD44-mediated uptake and inhibition of NF-κB-driven inflammatory and invasive programs. HA-guided niosomal sorafenib warrants *in vivo* validation as a selective nanotherapeutic strategy for OSCC.

▶ Please cite this article as:
Wu T, Li Y, Wang Z, Guo B. Hyaluronic acid-coated niosomal sorafenib targets CD44 and suppresses NF-κB signalling in oral squamous cell carcinoma. Iran J Basic Med Sci 2026; 29:

Introduction

Oral squamous cell carcinoma (OSCC) is increasingly being framed as an inflammation driven malignancy, in which NF-κB acts as a central hub. NF-κB is constitutively active in OSCC and drives the expression of IL-6, IL-8, CCL5, CXCL10, and matrix metalloproteinases, thereby fostering EMT, invasion, angiogenesis, and metastasis, features consistently associated with poorer outcomes in head and neck cancer. These mechanistic links have motivated strategies that either dampen NF-κB signaling directly or deliver therapeutics that suppress its upstream drivers (1).

Sorafenib, an oral multikinase inhibitor, targets RAF kinases and angiogenic receptor tyrosine kinases (VEGFR-2/-3, PDGFR-β), providing a pharmacologic rationale in NF-κB-high tumors where MAPK/ERK and pro-angiogenic cues converge. Beyond its canonical targets, sorafenib has shown synergy with ionizing radiation in OSCC models; in SAS/NF-κB-luc2 cells, it significantly heightened radiation-induced cytotoxicity and apoptosis, and suppressed radiation-induced NF-κB activity and downstream effectors. These data position sorafenib not only as an antiproliferative/anti-angiogenic agent but also as a functional NF-κB modulator in OSCC (2, 3).

To address the hydrophobicity and off-target toxicity of sorafenib, nano-delivery approaches have been explored. Among them, niosomes (nonionic surfactant vesicles) are attractive because of their scalable fabrication, stability, and capacity for hydrophobic payloads. A recent formulation using Span 60/Tween 60/cholesterol (45/45/10 mol %) demonstrated sustained release and enhanced *in vitro* efficacy versus free sorafenib (HepG2 model), highlighting niosomes as a promising platform to improve sorafenib's therapeutic window and pharmacodynamics, albeit most data to date are outside the OSCC setting (4).

The CD44-hyaluronan (HA) axis is particularly compelling for active targeting in OSCC. A 2023 meta-analysis reported that high CD44 expression predicts worse overall survival in OSCC (HR=1.71; 95% CI 1.18-2.47) and increases the risk of recurrence or death (HR=1.66; 95% CI 1.15-2.39), underscoring CD44's translational relevance as a dual biomarker and uptake handle. Consistent with this, HA-decorated nanocarriers have achieved superior cellular

***Corresponding author:** Bin Guo. Department of Stomatology, Central Hospital affiliated to Shandong First Medical University, No.105, Jiefang Road, Lixia District, Jinan, Shandong, 250013, China. Email: Likong071@gmail.com

uptake and antitumor activity in oral cancer models, and recent work has demonstrated CD44 engagement and enhanced lymphatic transport for HA-based nanoparticles carrying cytotoxics. Collectively, these data validate HA-guided targeting as a rational design principle for OSCC nanomedicine (5, 6).

Despite these advances, several methodological gaps limit previous studies and inform our design. First, many older "oral cancer" *in vitro* reports employed KB cells, now known to be misidentified HeLa derivatives, which compromises disease relevance; current best practice requires STR authentication and use of bona fide OSCC lines (e.g., CAL27, SCC-4, SCC-9). Second, even when sorafenib is nanoformulated, direct readouts of NF-**κB** pathway attenuation (e.g., p65 nuclear translocation and COX-2/MMP-9 transcription) are often missing, leaving mechanism-of-action inferences underpowered. Third, design-of-experiments (DOE), long-term colloidal stability, protein-corona effects (e.g., in 10% FBS), and like-for-like controls (empty/HA-free vesicles) have been inconsistently reported, which hinders reproducibility and translational assessment. Our approach is therefore structured to address these gaps explicitly: HA-coated niosomal sorafenib for CD44-mediated uptake, quantitative NF-κB target suppression (e.g., COX-2 and MMP-9), authenticated OSCC models, DOE-guided optimization, and stability/uptake assays under physiologically relevant serum conditions (7).

Finally, while the global cancer burden continues to rise (20 million new cases and 9.7 million deaths in 2022 across all cancers), OSCC remains disproportionately affected by inflammatory microenvironments and lifestyle cofactors, contexts in which targeted, mechanism-anchored delivery platforms are most likely to shift clinical outcomes (8). The accumulated evidence thus supports HA-guided niosomes as a credible strategy to potentiate sorafenib in OSCC by improving tumor-cell uptake and blunting NF-κB-driven programs, with clear next steps toward *in vivo* validation and comparative efficacy against standard-of-care combinations.

Materials and Methods

Materials

Sorafenib (chemical purity >99 %) was obtained from Bayer AG (Leverkusen, Germany). Span 60 (sorbitan monostearate, ≥98 %, CAS 1338-41-6, Sigma-Aldrich #S190500G), EDC/NHS, and cholesterol (ovine wool source) were purchased from Sigma-Aldrich (Germany) as nonionic surfactants and bilayer stabilizers, respectively. Hyaluronic acid (sodium hyaluronate, average Mw=100 kDa) was purchased from Sigma-Aldrich. Chloroform, methanol, and other solvents were of analytical grade. Phosphate-buffered saline (PBS, pH 7.4) was used as the hydration and dialysis medium. The CAL27 human oral squamous carcinoma cell line was obtained from the American Type Culture Collection (ATCC, CRL-2095). Dulbecco's modified Eagle's medium (DMEM) was obtained from Gibco, USA, and supplemented with 10 % fetal bovine serum (FBS) and 1 % penicillin-streptomycin. The experimental analysis of cells utilized three-(4-5-dimethylthiazol-2-yl)-2,5-diphenyl tetrazolium bromide (MTT)(Sigma), an Annexin V-FITC Apoptosis Detection Kit (Thermo Fisher Scientific), propidium iodide (PI) fluorescent dyes (Thermo Fisher Scientific), and TRIzol reagent for RNA extraction (Invitrogen). Bio-Rad supplied the cDNA synthesis kit and real-time PCR SYBR Green Master Mix. Analytical grade chemicals were used as received to prepare all the experimental solutions.

Preparation of sorafenib-loaded niosomes

Sorafenib-loaded niosomes were prepared by the thin film hydration method

Briefly, Span 60 (62 mg) and cholesterol (53 mg) were dissolved together (Span 60: cholesterol=1.15:1 mol mol^{-1}) with sorafenib (21 mg) in 10 ml of a chloroform:methanol mixture (2:1, v/v) in a round-bottom flask. The organic solvent was slowly evaporated under reduced pressure using a rotary evaporator at 58 ˚C (above the phase transition temperature of Span 60) to form a thin lipid-drug film on the flask wall. The dry film was then hydrated for 30 min at 50 ˚C with 10 ml of PBS (pH 7.4) with gentle shaking to yield multilamellar niosomal vesicles encapsulating sorafenib (9). The crude niosome suspension was subjected to size reduction by probe sonication (VCX-750 Ultrasonic Processor, 20 kHz) for 5 min in an ice bath at 40 % amplitude (110 W) for 5 min (3 sec on/5 sec off) to form nano-sized vesicles. Free sorafenib was removed by 24 hr dialysis (MWCO 10 kDa) against PBS at 4 ˚C and refreshed thrice. The pellet (sorafenib-loaded niosomes) was separated by ultracentrifugation at 20,000 rpm for 30 min, washed, and resuspended in PBS. The concentration of sorafenib in the niosomal suspension was determined by UV-Vis spectroscopy at λ_{max}=270 nm (the characteristic absorbance of sorafenib in DMSO) and compared against a calibration curve (Figure S1).

Hyaluronic acid coating by EDC/NHS coupling.

Sodium hyaluronate (1-2 mg) was dissolved in 0.10 M MES buffer (pH 5.5) to 1 mg ml^{-1} and gently stirred for 5 min. Carboxyl groups were activated with freshly prepared EDC·HCl and NHS at a molar ratio COOH:EDC:NHS=1:2:2 (for 2 mg HA: EDC 1.91 mg, 9.97 µmol; NHS 1.15 mg, 9.97 µmol) for 20 min at 22-25 ˚C (10). The activated HA solution was then added dropwise to aminated niosomes (total surfactant/lipid 5-10 mg in PBS, pH 7.4) under gentle stirring, and coupling proceeded for 2 hr at room temperature. Residual NHS esters were quenched by adding Tris (final concentration: 20 mM, 10 min). HA-coated niosomes were purified by ultracentrifugation (30,000 ×g, 30 min, 4 ˚C) and washed three times with PBS.

Box-behnken design (BBD) and response-surface analysis

In this study, the formulation of sorafenib-loaded niosomes (SOR@Nio) and HA-coated sorafenib-loaded niosomes (SOR@Nio/HA) was optimized using Design Expert software, employing a 3-factor, 3-level Box-Behnken design to evaluate the influence of three independent variables: drug content (Factor A), surfactant-to-cholesterol molar ratio (Factor B), and lipid-to-drug molar ratio (Factor C). The responses studied were particle size (Response 1), encapsulation efficiency (Response 2), and drug release (Response 3). The design comprised 15 experimental runs (Table 1), which were evaluated for their responses. As shown in Figure 1 Three factors, drug content (A), surfactant-to-cholesterol molar ratio (B), and lipid-to-drug molar ratio (C), were varied to determine their optimal levels for maximizing the desired properties of niosomal formulations.

Table 1. Screening runs from the Box-Behnken design (unoptimized). Vesicle size, entrapment efficiency (EE%), and polydispersity index (PDI) of different niosomal formulations containing sorafenib

		Factor 1	Factor 2	Factor 3	Response 1	Response 2	Response 3
Standard order	Run	A:Drug Content	B:Surfactant/Cholesterol	C:Lipid/Drug	Size	EE	Release
		mg	molar ratio	molar ratio	nm	%	%
2	1	20	1	30	180	86.52	91.44
4	2	10	2	30	230	85.84	89.26
3	3	5	1	30	250	50.25	60.13
1	4	20	1	10	195	77.1	80.72
6	5	5	1	10	183	80.19	71.75
7	6	20	1	20	280	69.57	70.42
5	7	5	2	20	247	61.55	70.59
8	8	10	0.5	20	232	67.12	73.21
10	9	5	1	20	224	58.32	64.14
9	10	10	2	10	230	79.16	87.93
12	11	10	2	20	256	73.18	87.66
11	12	20	1	20	218	81.63	85.19
13	13	10	0.5	30	201	81.84	75.67
15	14	10	0.5	10	210	79.26	72.82
14	15	10	1	20	248	80.91	71.93

Characterization of HA-coated sorafenib niosomes

Size and morphology of the formulation

The hydrodynamic size and PDI were measured by DLS (Malvern, 25 ˚C; backscatter 173˚; refractive index and viscosity set for water). The morphology was characterized by FE-SEM sputter-coated with Au/Pd; 5-10 kV (MIRA3 Tescan 3, Brno, Czech Republic), TEM negative staining with 1-2% uranyl acetate; 200 kV accelerating voltage (Philips EM208S) and topography (AFM) TriboScope® (USA) were measured on diluted dispersions tapping mode on mica; scan size 1-5 µm, scan rate 0.5-1.0 Hz. The surface charge of the nanoparticles (zeta potential) was measured using a Zetasizer (Malvern Instruments, Malvern, UK). FTIR (400-4000 cm^{-1}) confirmed components (Perkin Elmer 1720-X model - USA).

Drug EE and loading capacity

Sorafenib entrapment efficiency was determined by measuring the amount of free (unencapsulated) drug after niosome preparation. Briefly, SOR@Nio/HA suspensions were ultracentrifuged (40,000 rpm, 1 hr) to pellet the niosomes. The clear supernatant containing free sorafenib was collected, and its absorbance was measured at 270 nm. The concentration of sorafenib in the supernatant was calculated using a standard curve. EE% was calculated as:

$$Entrapment\ Efficiency\ (\%) = \left[\frac{A-B}{A}\right] \times 100 \quad \text{Eq. 1.}$$

Where A total amount of drug (or compound) initially added for encapsulation (mg), and B is the amount of free (non-encapsulated) drug found outside the nanoparticles

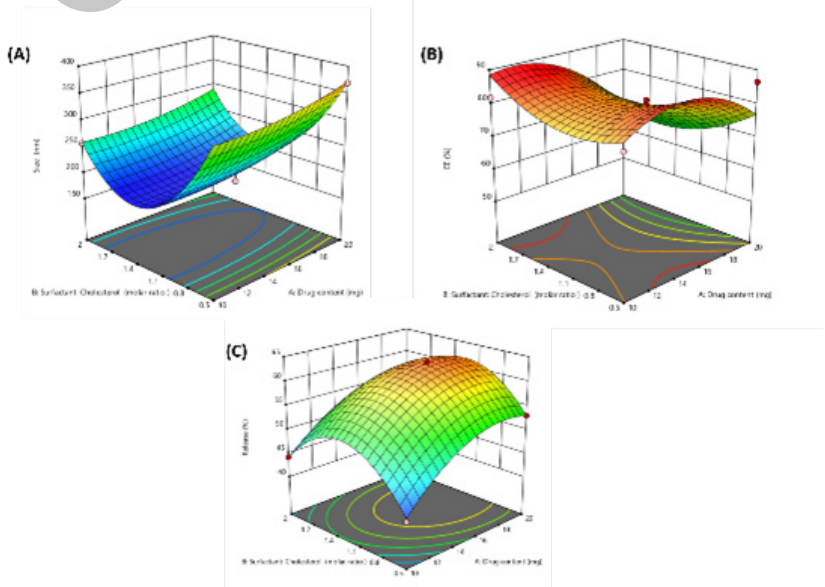

Figure 1. Three-dimensional response surface plots of niosomal formulations for A) size, B) EE, and C) 24 cumulative release as a function of the parameters (drug content and surfactant/cholesterol ratio)

(or the untrapped drug measured in the supernatant after centrifugation) (mg). Total sorafenib was defined as the amount of sorafenib added during hydration (20 mg). The experiments were performed in triplicate.

Drug loading (weight fraction)

$$DL\ (\%) = \frac{W\ encapsulated}{W\ vesicles} \times 100$$ Eq. 2. Drug loading (weight fraction)

Where $W_{encapsulated}$ is the mass of drug entrapped in the vesicles (mg), and $W_{vesicles}$ is the dry mass of the loaded vesicles (including surfactant, cholesterol, and drug solids; aqueous phase excluded)(mg).

Stability studies

SOR@Nio and SOR@Nio/HA were tested for 60 days at 25 ˚C and 4 ˚C. The average hydrodynamic size (defined as the Z-average), PDI, and EE of the dispersions were measured on days 15, 30, and 60 after the synthesis date and compared with the results obtained immediately after the synthesis. It is noteworthy that the samples were kept undisturbed (without any shaking or mixing) during the stability test, which was different from the release study conditions.

In vitro drug release study and kinetic modelling

The release was measured by dialysis (MWCO 12 kDa) at 37 ˚C with gentle orbital shaking (100 rpm) under sink conditions. Donor was 2.0 ml vesicle dispersion (sorafenib, SOR) sealed in dialysis tubing. The receiver was 50 ml of buffer. Two media were used: PBS, pH 7.4, 150 mM NaCl, and acetate buffer, pH 5.5, 150 mM NaCl (to mimic endolysosomal pH). At preset times (0.5, 1, 2, 4, 6, 12, 24, 36, and 48 hr), 1 ml was withdrawn and replaced with fresh medium; concentrations were quantified by UV-Vis spectroscopy. The cumulative release (%) was corrected for volume withdrawal.

Cell culture and MTT assay

CAL27 cells were seeded at 5.0×10^3 cells/well in 96-well plates (100 µl/well) and incubated for 24 hr in DMEM complete medium at 37 ˚C in a humidified atmosphere with 5% CO_2. Treatments (free SOR, niosomal SOR (SOR@Nio), HA-coated niosomal SOR (SOR@Nio/HA)) were added in 100 µl complete medium for 48 hr across 8 concentrations bracketing the expected IC_{50} (e.g., 0.5-64 µM for free SOR; niosomal groups adjusted to SOR-equivalent concentrations). Final DMSO≤0.10% (v/v) in all wells. Controls: vehicle (0.10% DMSO), blank niosomes, blank Nio/HA, and positive cytotoxic control (staurosporine 1 µM, 4 hr). After treatment, MTT (0.5 mg ml^{-1}, 20 µl) was added for 3-4 hr; formazan was dissolved in DMSO 100 µl; A_{570}-A_{630} was read. Viability (%) was normalized to that of the vehicle.

The absorbance at 570 nm (with a 630 nm reference) was measured using a microplate reader (AccuReader, Metertech, Taiwan) at 570 nm (11). Cell viability was reported as follows:

$$Cell\ viability\ (\%) = \frac{OD_{570}\ sample}{OD_{570}\ control} \times 100$$ Eq.3. Cell viability (MTT)

The percentage of cell viability was calculated relative to the untreated control cells (100 % viability). Dose-response curves were plotted, and the half-maximal inhibitory concentration (IC_{50}) for each formulation in each cell line was determined using nonlinear regression analysis. Each experiment was independently repeated three times.

Apoptosis analysis by annexin V/PI dual staining

CAL27 cells (1.2×10^5 per well; 12-well; 1 ml) were treated for 24 hr at 0.5×/1×/2× IC_{50} (free SOR 11.8±1.1 µM; SOR@Nio/HA 5.2±0.9 µM); controls were 0.10% DMSO, blank niosomes, blank Nio/HA, and staurosporine 1 µM (4 hr). After treatment, Annexin V-FITC/PI staining (manufacturer's protocol) was analyzed on a BD FACSCanto II with single-stained compensation, collecting ≥10,000 events/sample; gating included singlets to live/dead to Annexin/PI quadrants, and early, late, and total (Q2+Q3) apoptosis (%) were reported. A 24 hr window captured early apoptotic events, whereas 48 hr MTT quantified cumulative viability. For gene expression, total RNA (TRIzol; A260/280=1.9-2.1) was reverse-transcribed from 1 µg RNA (random hexamers, 20 µl cDNA), and SYBR Green qPCR (QuantStudio; 95 ˚C 2 min; 40×: 95 ˚C 15 sec/60 ˚C 60 sec; single-peak melt) with primer efficiency 90-110% (R^2≥0.99) was performed. Expression was normalized to GAPDH (validated with ACTB) and analyzed by $2^{-\Delta\Delta Ct}$ (vehicle=1.0) for BTG3/COX-2, MMP9, BAX, BCL-2, and RELA (p65); primer sequences are listed in Table S2.

DAPI staining

The morphological features of the cell nuclei were evaluated using fluorescence microscopy following DAPI (4′,6-diamidino-2-phenylindole; D9542, Sigma-Aldrich) staining. CAL27 oral squamous carcinoma cells were exposed for 24 hr to vehicle (0.10% DMSO), blank niosomes, SOR@Nio, or SOR@Nio/HA at their working sorafenib-equivalent concentrations. Then, they were washed with PBS (pH=7.4) three times, followed by fixation with ice-cold 70% ethanol, resuspension in DAPI (0.5 µg/ml), and 15 min of incubation at 37 ˚C in the dark. Fluorescence microscopy (Eclipse Ti, Nikon Instruments Inc., New York, USA) was then used to examine the cells under identical exposure and gain settings.

Statistical analysis

Data are expressed as mean±standard deviation (SD). GraphPad Prism 9.0 and Origin Pro 2018 were used for statistical analyses. For comparisons between multiple groups, one-way or two-way analysis of variance (ANOVA) was performed, followed by Tukey's *post hoc* test for pairwise comparisons. All experiments were repeated at least three times to ensure reproducibility.

Results

Optimization of formulation by design expert

A 3-factor/3-level Box-Behnken design (Design-Expert) probed the effects of drug load (A), surfactant:cholesterol (B), and lipid:drug (C) on size, EE, and 48 hr release (n=15; Table 1). Drug load and B were the dominant terms. An operating window at A=10-12 mg and B≥1:1 produced approximately 200 nm vesicles with an EE of approximately 86.3% and controlled release (50%/48 hr). The detailed models and statistics are provided in the S1. Main-effect trends indicated that increasing A (drug content) and decreasing B (cholesterol fraction) enlarged the vesicles,

consistent with higher bilayer loading and reduced membrane rigidity at low cholesterol levels. C (sonication time) exhibited a negative slope for size and PDI up to the center level, reflecting the shear-mediated breakup of larger multilamellar structures; beyond the upper level, diminishing returns were observed. For EE, both A and B showed positive contributions with a significant A×B interaction, suggesting that adequate surfactant capacity, together with membrane order, is required for maximal drug retention. From a mechanistic standpoint, the cholesterol window that minimizes size while preserving a high EE is consistent with vesicle mechanics: excessive cholesterol can suppress bilayer permeability, but also stiffen membranes, hampering efficient size reduction during sonication; too little cholesterol softens the bilayer, increasing the likelihood of fusion and drug leakage. The observed A×B synergy for EE accords with the requirement of sufficient surfactant density to solubilize hydrophobic sorafenib while maintaining membrane order to prevent diffusion-driven escape.

Size and morphology by microscopic analysis (SEM, TEM, AFM)

Various characterization techniques, including Scanning Electron Microscopy (SEM), Atomic Force Microscopy (AFM), TEM, DLS, and Polydispersity Index (PDI), were employed to fully characterize the physicochemical properties and morphologies of sorafenib-loaded nanoniosomes (SOR@Nio/HA, SOR@Nio, and Nio, which are blank niosomes)(Figure S2). Average hydrodynamic diameter measured by DLS was 177±8 nm, PDI=0.23±0.02 (n=3), indicating moderate monodispersity based on the literature (12). ZetaPotential shifted from −8.5±0.4 mV to −22.1±0.6 mV after HA coating, confirming surface functionalization. TEM images of negatively stained vesicles revealed spherical particles (170 nm) with an electron-dense core (scale bar=100 nm). FESEM images of SOR@Nio and SOR@Nio/HA are shown in Figure 2. The niosomal size distributions measured by FESEM were 173 and 209 nm for SOR@Nio and SOR@Nio/HA, respectively, which aligned with the optimal size for cellular uptake via endocytosis (13). FESEM surface analysis revealed spherical nanoparticles with a smooth surface, which is typical of nanoniosomes. The HA-coated formulation (SOR@Nio/HA) showed a more homogeneous surface than the uncoated SOR@Nio, indicating the stabilizing effect of the hyaluronic acid layer (14).

TEM analysis provided high-resolution imaging of the internal structure of the nanoparticles. TEM micrographs revealed a well-defined core-shell structure for the SOR@Nio/HA nanoparticles, where the core was composed of SOR@Nio and the surrounding shell was identified as the hyaluronic acid coating. This core-shell structure is intended to maintain sorafenib's stability and ensure controlled release, preventing premature drug leakage during circulation. The particle sizes of SOR@Nio and SOR@Nio/HA observed by TEM were 160 and 210 nm, respectively, which is in good agreement with the DLS measurements, confirming the uniformity of the nanoparticles (9). The presence of the HA layer was further confirmed by the TEM images, which demonstrated distinct separation between the core and shell.

Tapping-mode AFM on mica (scan size 1-5 μm; 0.5-1.0 Hz) showed isolated vesicles and small clusters with uniform lateral profiles (Figure 3). Single-particle height analysis (n=50) yielded a median height of 22 nm IQR 17-27 nm for Opt-F, consistent with substrate-induced flattening of soft vesicles on mica. Occasional higher features (approximately 60 nm) coincided with particle overlaps or multilamellar patches and were excluded from statistics using an artifact filter (non-circularity >0.35 and abrupt height discontinuities). The lateral dimensions did not show tip-induced smearing at the chosen scan rates.

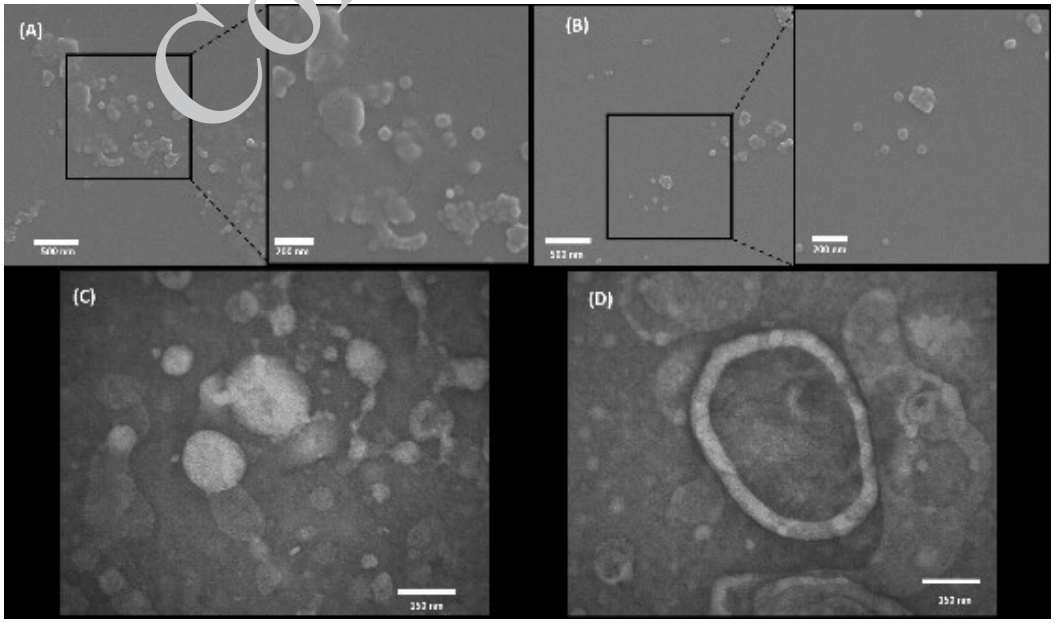

Figure 2. Electron microscopy (SEM) images of sorafenib-loaded nanoniosomes
(A) SEM image showing the overall morphology of the sorafenib-loaded niosomes, with a size distribution centered around 500 nm for SOR@Nio and (B) for SOR@Nio/HA. These figures provide a higher magnification image (200 nm scale), highlighting the individual niosomal particles. (C) TEM image of SOR@Nio as a closer view of the niosomes, revealing a uniform and spherical shape with some variability in size. (D) TEM image of SOR@Nio/HA at a higher magnification of a representative niosome, showing its well-defined surface and structural integrity. The scale bars in each panel correspond to 500 nm (A and B) and 150 nm (C and D)

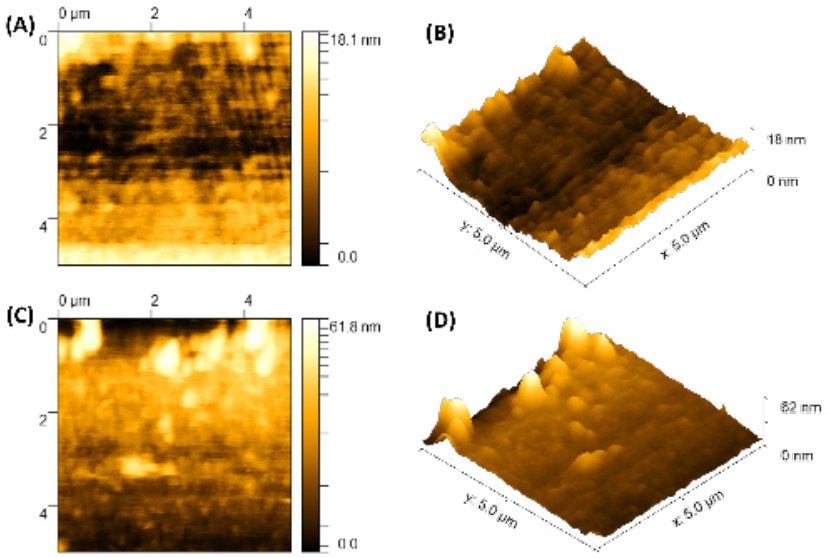

Figure 3. Atomic force microscopy (AFM) images of sorafenib-loaded nanoniosomes
Panel (A, B) shows the 2D AFM image and the corresponding 3D height profile of SOR@Nio, in which a smooth uniform topography with a height variation of 18 nm was observed. The inset in the 3D image shows the surface structure of the nanoparticle at high-resolution. The bottom panel (C, D) displays a higher magnification 2D AFM image and 3D profile

Particle dispersity index, size and surface charge

The sorafenib-loaded niosomes were nanometer-scale in size, with a relatively narrow distribution. DLS showed that SOR@Nio had an average hydrodynamic diameter of 150.8±5.8 nm with PDI=0.218±0.010, indicating a uniform population. After coating with HA, the mean diameter increased to 177.4±8.3 nm (PDI=0.256±0.015), reflecting the adsorbed polymer layer on the vesicle surface. This slight increase in size upon surface decoration is consistent with previous reports on polymer- or ligand-coated niosomes. Additional DLS-based particle size analyses are provided in the Supporting Information (Figure S2). These results confirmed narrow and monodisperse distributions, with hydrodynamic diameters centered around 150 and 177 nm, further supporting the stability and uniformity of the nanocarrier formulations. For instance, Moammeri *et al.* observed an increase in the size of niosomes from 184 to 192 nm when they were functionalized with folate-PEG. Our HA-coated niosomes remained well within the sub-200 nm size range, which is favorable for cellular uptake and tumor penetration. The zeta potential of uncoated sorafenib niosomes was measured as -8.5±0.4 mV, likely due to the presence of deprotonated fatty acid groups or sorafenib molecules at the particle surface. Upon HA coating, the zeta potential shifted to -22.1±0.6 mV (net change of -13.6 mV), confirming the successful adsorption of the anionic HA on the vesicle surface. As shown in Table 2, a strongly negative zeta potential enhances colloidal stability owing to electrostatic repulsion, which is advantageous for preventing aggregation during storage and in biological media. The high magnitude of the negative surface charge observed (comparable to the-38 mV reported for similar HA-coated niosomes) suggests a stable formulation. Zeta potential values below -20 mV are typically sufficient to confer electrostatic stability in suspension (15).

EE and drug loading

Entrapment efficiency was quantified by an indirect method after separating free sorafenib from vesicles via ultracentrifugation at 30,000×g, 30 min, 4 ˚C/100 kDa centrifugal ultrafiltration. The supernatant (free drug) was diluted 1:10 in EtOH:water 70:30/ACN:water 60:40 and read at λ_{max}=270 nm. A ten-point calibration curve spanning 1-40 µg ml^{-1} yielded $R^2 \geq 0.999$. The optimized formulation achieved a validated EE of 85.6-87.2 % (mean±SD 86.3±0.5 %, n=3), with a mass balance of 98-101%, indicating minimal processing losses. Mechanistically, moderate cholesterol maintains sufficient membrane rigidity to limit back-diffusion while avoiding excessive stiffening that would reduce bilayer accommodation of hydrophobic sorafenib-consistent with the significant A×B interaction found in the response-surface analysis.

For the optimized formulation, DL=7.2±0.4 % (w/w), corresponding to 0.072±0.004 mg sorafenib per mg vesicle (total surfactant+cholesterol+drug solids). Notably, HA grafting did not significantly change the EE relative to that of non-coated niosomes (P>0.05), consistent with coupling occurring predominantly at the corona without disrupting the bilayer core. However, prolonged storage at 25 ˚C caused a gradual decrease in EE (e.g., -12% at day 60), whereas storage at 4 ˚C maintained ≥ 90 % of the initial EE, matching the PDI trends and suggesting fusion-assisted leakage at higher temperatures.

Table 2. Zeta potential measurements of sorafenib-loaded nanoniosomes (SOR@Nio) and hyaluronic acid-coated sorafenib-loaded nanoniosomes (SOR@Nio/HA) at different pH values

Formulations	Zeta Potential	
	pH 5.2	pH 7.4
SOR@Nio/HA	-36.8±0.8	-22.1±0.6
SOR@Nio	-27.1±0.5	-8.5±0.4

Zeta potential values of SOR@Nio and SOR@Nio/HA formulations were measured at pH 5.2 and pH 7.4, to assess the colloidal stability and surface charge characteristics of the nanoparticles under varying physiological conditions

Fourier-transform infra analysis result

As shown in Figure 4, SOR@Nio/HA represents a broad band at 3443 cm^{-1} corresponding to O-H stretching (from HA's hydroxyl groups), with its broadness indicating hydrogen bonding. Peaks at 2927 and 2853 cm^{-1} (C-H stretches of aliphatic chains) were observed from the lipid/surfactant components (and possibly sorafenib's aliphatic moieties). The broadness of this peak indicates the presence of hydrogen bonds. Two other peaks at 2927 cm^{-1} and 2853 cm^{-1} are indicative of C-H stretching vibrations from aliphatic hydrocarbons, likely corresponding to the niosome and sorafenib molecule. HA exhibited strong bands at 1610 cm^{-1} (antisymmetric COO − stretch) and 3400 cm^{-1} (O-H stretch). In the SOR@Nio/HA spectrum, characteristic peaks at 1654 cm^{-1} (amide I), 1542 cm^{-1} (amide II), and a broad band at 3280 cm^{-1} (O-H stretch) confirmed successful HA coating. The presence of sorafenib's aromatic peaks (e.g., a peak at 1575 cm^{-1}) overlapping with the Span 60/cholesterol and HA bands indicated the presence of the drug in the spectra. A slight shift in the carbonyl stretching frequency of sorafenib was observed (from 1680 to 1674 cm^{-1}), which may suggest weak hydrogen bonding or physical interactions between sorafenib and the lipid or HA components. Importantly, the HA signature peak at 1610 cm^{-1} was still visible in the coated niosomes, confirming the HA coating. No new peaks or major shifts were observed, implying that sorafenib is encapsulated primarily through non-covalent, physical entrapment rather than chemical bond formation, a desirable outcome to ensure drug integrity. The 1560 cm^{-1} peak could represent N-H bending vibrations, potentially from the sorafenib molecule or HA interactions.

In the sorafenib (free drug) sample, a broad band around 3307 cm^{-1} was observed, attributable to overlapping N-H and O-H stretching vibrations, particularly in the imidazole ring. The presence of a similar peak in the SOR@Nio/HA spectrum suggests that the functional groups of the drug remained intact during the formulation. Another peak at 1725 cm^{-1} represents the C=O stretching of the carboxyl group in the sorafenib molecule, confirming the drug's

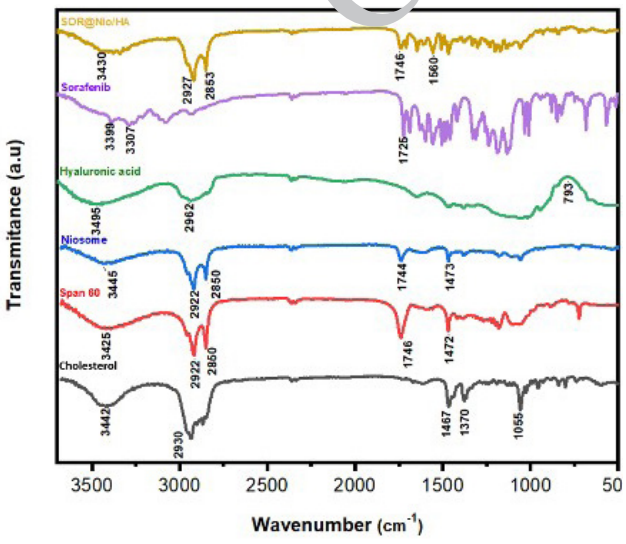

Figure 4. FTIR spectra of sorafenib-loaded nanoniosomes (SOR@Nio/HA), uncoated niosomes (SOR@Nio), sorafenib, hyaluronic acid, niosome, span 60, and cholesterol

structure. HA represents a broad band characteristic of O-H stretching at 3445 cm^{-1}, which suggests the presence of hydroxyl groups from HA. The peaks at 2922 cm^{-1} and 2850 cm^{-1} correspond to C-H stretching vibrations, likely from the saccharide backbone of hyaluronic acid. The peak at 793 cm^{-1} is a C-H bending vibration likely associated with the polysaccharide structure of HA.

In niosomes (empty carrier), we can see a broad band at 3445 cm^{-1} due to O-H stretching vibrations, likely from the residual hydroxyl groups in the lipid bilayer. The peaks at 2922 cm^{-1} and 2850 cm^{-1} represent C-H stretching vibrations from the alkyl chains of the surfactants used to form the niosomes. The peak at 1744 cm^{-1} represents the C=O stretching vibration from ester groups in the surfactant molecules, such as Span 60. In addition, the peak at 1473 cm^{-1} corresponds to CH_2 bending vibrations, further confirming the presence of surfactant molecules. For Span 60, the peak at 1746 cm^{-1} represents the C=O stretching vibration and is attributed to the ester group in Span 60, a surfactant used in the niosome formulation. In addition, at 1472 cm^{-1}, the CH_2 bending vibration was consistent with the surfactant structure. At 2922 cm^{-1}, there is a sharp band corresponding to C-H stretching vibrations in the hydrophobic alkyl chains of Span 60. For cholesterol, the broad peak at 3442 cm^{-1} is associated with O-H stretching from the hydroxyl group of cholesterol. The peaks at 2930 cm^{-1} and 2850 cm^{-1} correspond to C-H stretching vibrations of the alkyl chains of cholesterol. The peak at 1467 cm^{-1} corresponds to C-H bending, typical of the hydrocarbon tail of cholesterol.

The peaks for C-H, O-H, and C=O stretching were observed in all the components of the formulation. The shift or overlap of these peaks in the SOR@Nio/HA spectrum compared to the individual components suggests the successful incorporation of both sorafenib and hyaluronic acid into the niosome formulation. The appearance of peaks related to the O-H and C-H stretching of HA in the SOR@Nio/HA formulation suggests that hyaluronic acid may be interacting with the drug or surfactant, which is typical in such formulations designed for receptor-mediated drug delivery. The presence of ester-based peaks in the niosome formulation at 1744 cm^{-1} and 1473 cm^{-1} confirms that the niosomes are composed of surfactant molecules such as Span 60 and cholesterol, which are essential for the formation of stable lipid bilayers. The similarity between the C-H and C=O stretching vibrations in the niosome, Span 60, and cholesterol spectra confirmed that lipid carriers are likely to provide a stable environment for the encapsulation of sorafenib. FTIR analysis confirmed the successful formulation of sorafenib-loaded niosomes with hyaluronic acid coating (SOR@Nio/HA).

Thermal behavior of the HA coating

TGA under N_2 (10 ˚C min^{-1}) corroborated HA grafting and its impact on vesicle robustness. Blank niosomes showed bound-water loss below 100-130 ˚C (Δm=2-5%), a main surfactant/cholesterol degradation at 280-330 ˚C (Δm=55-65%), and 3-8% residue at 600 ˚C. Sorafenib loading slightly shifted the main DTG maximum by increasing 5-15 ˚C and reduced low-temperature loss by 0.5-1%, consistent with bilayer densification. HA coupling (HA-Nio-SOR) increased low-temperature loss to 3-6% and introduced a DTG shoulder at 240 ˚C (HA dehydration/decarboxylation),

Table 3. Thermogravimetric parameters of hyaluronic acid (HA) and HA-coated sorafenib-loaded niosomes (HA-Nio-SOR)

Sample	Tonset (˚C)	T_{50} (˚C)	Residue 800 ˚C (%)
HA	245±2	390±4	39.8±0.6
HA-Nio-SOR	270±3	415±5	13.1±0.3

HA-Nio-SOR exhibited a higher degradation onset (Tonset) and lower final residue than native HA, indicating the enhanced thermal stability and full organic composition of the nanocarrier system

raising the 200-350 ˚C mass-loss budget by increasing 4-9% vs Nio-SOR (Table 3). After correcting for drug content, this increment corresponded to 5-12 µg HA per mg vesicle, in agreement with the uronic-acid assay (±10-15%); residue at 600 °C rose by 1-3% (Figure 5).

Stability study of formulation

As shown in Figure 6, over 60 days, both SOR@Nio and SOR@Nio/HA were stable at 4 ˚C, but showed temperature-sensitive increases in size and PDI at 25 ˚C. For SOR@Nio, mean size rose (4 ˚C: 177 to 283 nm; 25 ˚C: 192 to 320 nm) with PDI 0.22-0.25 at 4 ˚C vs 0.32 at 25 ˚C. HA-coated vesicles were more heat-sensitive (4 ˚C: 276 to 319 nm; 25 ˚C: 280 to 337 nm), with PDI 0.27 to 0.36 (4 ˚C) and 0.28 to 0.42 (25 ˚C; P<0.05, day 60). EE for SOR@Nio stayed 86 to 85% at both temperatures, whereas SOR@Nio/HA was stable at 4 ˚C (82%) but declined at 25 ˚C (84.4 to 79.2%, P<0.05).

In vitro release behavior

HA-coated sorafenib niosomes displayed sustained, pH-dependent release. At pH 7.4, 30% was released in 24 hr and 55% by 5 days; at pH 5.5, 45.1±2.2% was released in 24 hr (29.7±1.8% at 7.4; n=3, P<0.01) and >90% by 50 hr. As shown in Figure 7, profiles were biphasic (0.6 hr burst then diffusion-controlled plateau): the burst was strongest at pH 5.5 (48% in 6 hr), whereas at pH 7.4 release remained 30% over the experiment. Uncoated SOR@Nio were tighter at both pH values; the presence of HA and acidity together accelerated diffusion (1.3× amplification with HA). Bian *et al.* achieved 80 % release from lactosylated pH-responsive nanoparticles at pH 5.5 versus <60% at pH 7.4, but their neutral pH leakage remained twice as high as in our HA-coated system (16). Polymer-grafted (poly acrylic-acid) niosomes reported by Saharkhiz *et al.* liberated 80%, 60%, and 40% of curcumin at pH 4.0, 6.5, and 7.4, respectively, numerically close to our values, yet achieved with a synthetic, non-biorecognisable shell (17). Kinetic fitting to zero-, first-order, Higuchi, and Korsmeyer-Peppas favored Higuchi/K-P under acidic conditions (R^2>0.9); n=0.42-0.59 indicated a shift from Fickian (7.4) to anomalous (diffusion+erosion) transport (5.5)(Table 4, Figure S3).

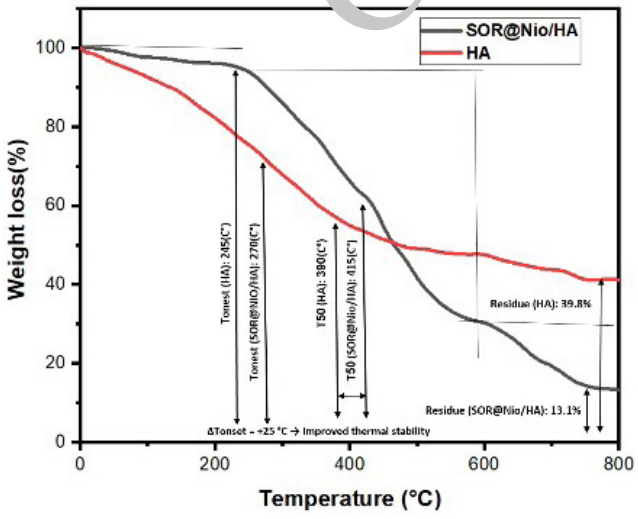

Figure 5. Thermogravimetric analysis (TGA) curves of hyaluronic acid (HA) and HA-coated sorafenib-loaded niosomes (HA-Nio-SOR)
HA-Nio-SOR showed a higher degradation onset (270 ˚C) than pure HA (245 ˚C), indicating enhanced thermal stability due to HA-niosome interactions

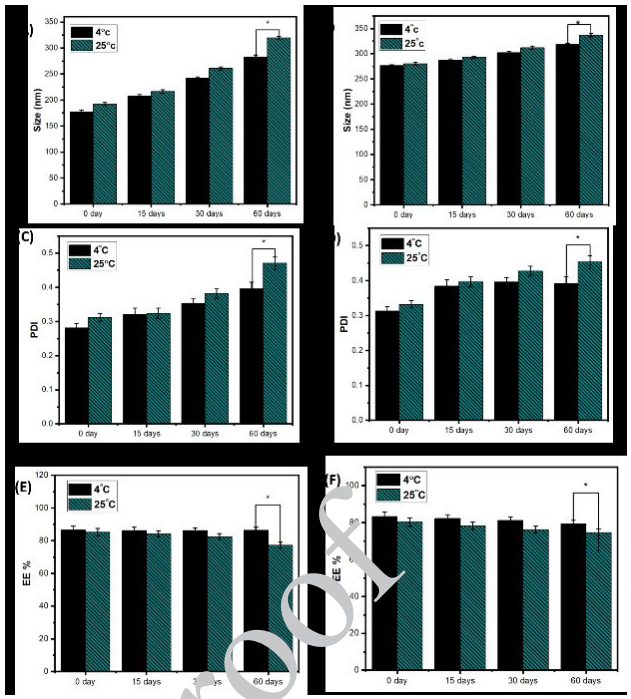

Figure 6. Stability, particle size, polydispersity index (PDI), and encapsulation efficiency of sorafenib-loaded nanoniosomes (SOR@Nio) and hyaluronic acid-coated nanoniosomes (SOR@Nio/HA) at 4 ˚C and 25 ˚C over 60 days
This figure shows the stability of the SOR@Nio and SOR@Nio/HA formulations stored at 4 ˚C and 25 ˚C for 60 days. The particle size distribution (top) and PDI (middle) and encapsulation efficiency (bottom) at 25 ˚C (P<0.05 vs 4 ˚C at day 60)

Cytotoxicity of sorafenib nanoniosomes in OSCC cells

The cytotoxic effects of the sorafenib nanoformulations on CAL27 cells were evaluated. Figure 8 depicts the cell viability of CAL27 cells after 48 hr of treatment with

Table 4. Drug release kinetic parameters of sorafenib-loaded nanoniosomes (SOR@Nio) and hyaluronic acid-coated sorafenib-loaded nanoniosomes (SOR@Nio/HA) at different pH values

Formulations	Zero- order	First- order	Higuchi	Korsmeyer-Peppas	
	R^2	R^2	R^2	R^2	n
SOR@Nio/HA (pH 5.2)	0.6932	0.6272	0.9189	0.9235	0.2423
SOR@Nio/HA (pH 7.4)	0.7326	0.5149	0.8231	0.8185	0.5748
SOR@Nio (pH 7.4)	0.731	0.5393	0.8464	0.5096	0.0156
SOR@Nio (pH 5.2)	0.6899	0.6275	0.9206	0.6411	0.0045

The table presents the regression coefficients (R^2) for various kinetic models (Zero-order, First-order, Higuchi, and Korsmeyer-Peppas) describing the drug release profiles of SOR@Nio and SOR@Nio/HA formulations at pH 5.2 and pH 7.4

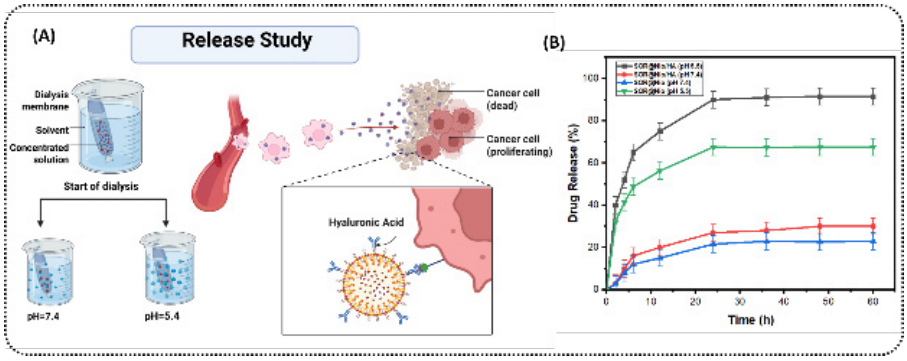

Figure 7. Drug release profile of sorafenib-loaded nanoniosomes (SOR@Nio) and hyaluronic acid-coated sorafenib-loaded nanoniosomes (SOR@Nio/HA) (A) Schematic overview of the in vitro drug release study performed through dialysis membranes, in which sorafenib-loaded nanoformulations (SOR@Nio and SOR@Nio/HA) were positioned in a solvent solution at two different pH values (pH 7.4 and pH 5.5). The release profile of sorafenib was assessed over time, focusing on how the pH influenced drug release and whether the HA receptor (CD44) could help in targeting cancer cells. (B) Release profiles of cumulative drug release (%) are plotted vs time (hours) for the SOR@Nio with and without HA at pH 7.4 and pH 5.5 At pH 5.5, the release of sorafenib was remarkably higher, indicating a pH-sensitive release profile of the HA-coated formulation (SOR@Nio/HA) in contrast to the uncoated formulation (SOR@Nio). Data are presented as mean±SD of triplicate measurements

increasing concentrations of sorafenib (0-50 μM) in different formulations. All sorafenib treatments produced a dose-dependent reduction in CAL27 cell viability, whereas blank niosomes (with or without HA) showed no significant toxicity (cell viability remained at 98 % at the highest particle concentration equivalent to 50 μM drug, confirming the biocompatibility of the niosomal carriers). Free sorafenib had an IC_{50} of 11.8±1.1 μM against CAL27 cells. IC_{50} values (non-linear four parameter fit, GraphPad, 95 % CI) were 11.8 μM, 7.4 μM, and 5.2 μM for free SOR, SOR@Nio, and SOR@Nio/HA, respectively (n=3). Thus, the HA-Nio formulation was approximately 2.4-fold more effective than the free drug at inhibiting CAL27 cell growth (P<0.01).

In line with previous studies, which will be mentioned in the discussion, our HA-coated sorafenib niosomes reduced the CAL27 IC_{50} from 11.8±1.1 μM (free SOR) to 5.2±0.9 μM (2.3× improvement; MTT, n=3), confirming enhanced anti-proliferative activity.

Modulation of NF-κB pathway, inflammatory mediators, and apoptotic axis

CAL27 cells were treated for 24 hr at 1×IC_{50} with vehicle (0.1% DMSO), blank niosomes, blank HA-niosomes, free SOR, Nio-SOR, HA-Nio-SOR (Opt-F); gene expression was quantified by qRT-PCR, normalized to GAPDH (validated with ACTB) and analyzed by $2^{-\Delta\Delta Ct}$ (mean±SD, n=3). As shown in Figure 9, versus vehicle, HA-Nio-SOR

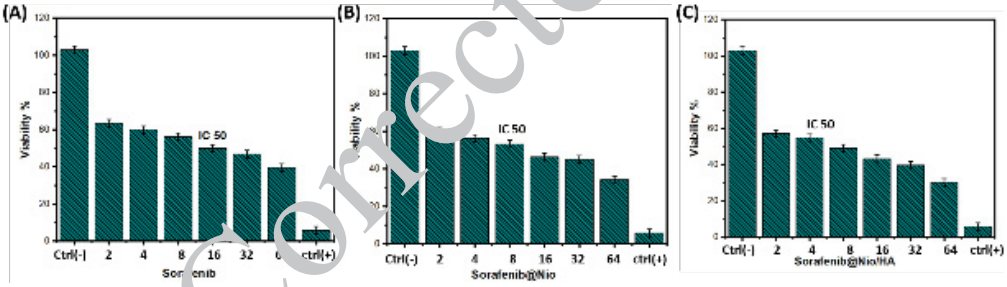

Figure 8. *In vitro* cytotoxicity assessment of free sorafenib and sorafenib-loaded niosomal formulations against cancer cells after 48 hr incubation was evaluated by MTT assay
(A) Dose-dependent cell viability after treatment with free sorafenib. (B) Cytotoxic effect of sorafenib-loaded niosomes (SOR@Nio) without hyaluronic acid (HA) modification. (C) Cytotoxicity of hyaluronic acid-decorated sorafenib-loaded niosomes (SOR@Nio/HA). IC_{50} values indicate the concentration required to reduce cell viability by 50%, demonstrating enhanced cytotoxicity for HA-modified niosomes compared to both non-modified vesicles and free drug. Data are presented as the mean±SD (n=3)

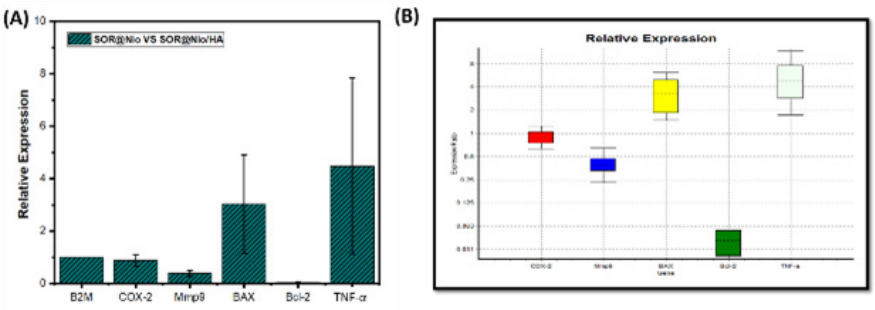

Figure 9. Relative mRNA expression of COX-2, MMP-9, BAX, Bcl-2, and TNF-α in CAL27 cells treated with SOR@Nio/HA relative to SOR@Nio, quantified as $2^{-\Delta\Delta Ct}$ (values >1 indicate up-regulation)
BAX and TNF-α are up-regulated, whereas Bcl-2, MMP-9, and COX-2 are down-regulated; B2M (housekeeping gene) remains =1. Data are mean±SD (n=3). In panel B, the y-axis is logarithmic. P<0.05, P<0.01 vs SOR@Nio

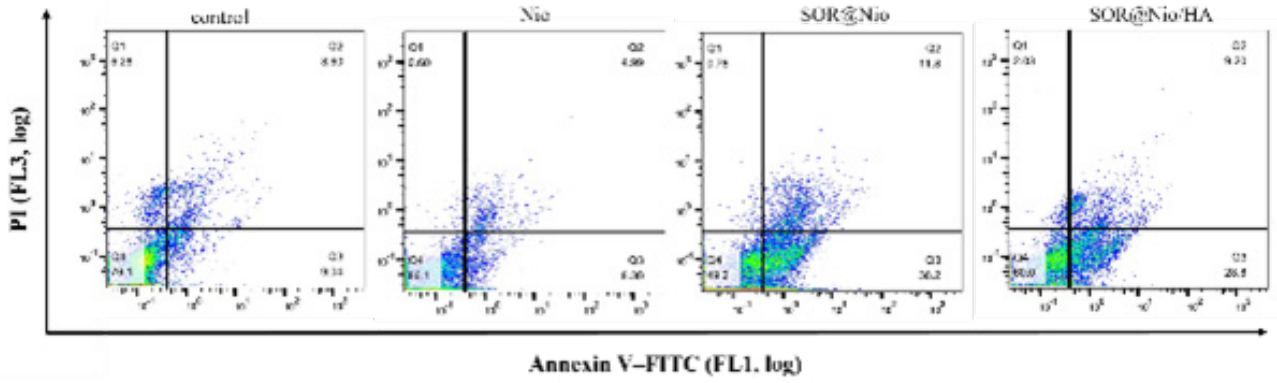

Figure 10. Flow-cytometry analysis of apoptosis in CAL27 cells treated with different sorafenib formulations for 24 hr and stained with Annexin V-FITC and PI
Dot plots represent (A) untreated control, (B) blank niosomes (Nio), (C) free sorafenib (SOR), and (D) HA-coated sorafenib-loaded niosomes (HA-Nio-SOR)

markedly reduced PTGS2/COX-2 to 0.35±0.05-fold and MMP9 to 0.32±0.06-fold (one-way ANOVA $P<0.001$; Tukey vs vehicle $P<0.001$), exceeding the reductions seen with free SOR (0.62±0.08) and Nio-SOR (0.48±0.07)($P<0.01$ and $P<0.05$, respectively). TNF-α also decreased (0.58±0.09-fold, $P<0.05$), and under a TNF-α challenge (10 ng ml^{-1}; 2 hr pretreat) HA-Nio-SOR blunted the inducible rise of COX-2/MMP-9 by 45-60% vs challenged vehicle (interaction $P<0.01$). Concomitantly, BAX increased (1.6±0.2-fold) while BCL-2 decreased (0.55±0.08-fold), yielding a BAX/BCL-2 ratio of 2.9±0.5 (vehicle = 1.0) that correlated with Annexin V/PI apoptosis at 24 hr (r=0.70). RELA/p65 remained 0.9–1.1-fold (ns), consistent with predominantly post-translational NF-κB control (Figure S4, S5 and Table S1, S2).

Apoptosis induction by annexin V/PI staining

Flow-cytometric Annexin V–FITC/PI (24 hr; Figure 10) showed low basal apoptosis in controls (Q3 9.0%, Q2 8.6%, Q4 76.1%; Q1 6.3%). Blank niosomes were biocompatible (Q3 8.3%, Q2 5.0%; viability 86.1%). Free sorafenib induced the highest total apoptosis (50.0%: Q3 38.2%, Q2 11.8%). HA-Nio-SOR yielded 38.0% total apoptosis (Q3 28.8±2.4%, Q2 9.2±1.1%; $n=3$), significantly higher than control/blank and lower than free SOR ($P<0.05$ vs control/blank; $P<0.01$ vs free SOR). Necrosis (Q1) remained ≤2% in treated groups (Figure 10).

Effects of nanoformulation on nuclear characteristics

DAPI (4′,6-diamidino-2-phenylindole) staining revealed clear, treatment-dependent nuclear changes in CAL27 cells after 24 hr (Figure 11). Vehicle and blank (Nio / HA-Nio) groups showed dense fields of uniform, round/oval nuclei, whereas SOR@Nio and SOR@Nio/HA displayed numerous nuclei with bright chromatin condensation, margination at the nuclear rim, and fragmented/pyknotic bodies, hallmarks of apoptosis. Images were acquired with identical exposure/gain; scale bar=100 µm.

Discussion

In this study, SEM/TEM/AFM corroborates the compact, narrowly dispersed vesicle population identified by DLS, and the expected hierarchy TEM (number-weighted) was smaller than DLS (intensity-weighted), supporting the physical interpretation of the hydrated corona and drying effects. From a translational perspective, maintaining a sub-200-nm size with a low PDI is advantageous for tumor penetration and colloidal stability. The microscopy results thus validated the morphological quality of Opt-F used for downstream release, cytotoxicity, and NF-κB-axis

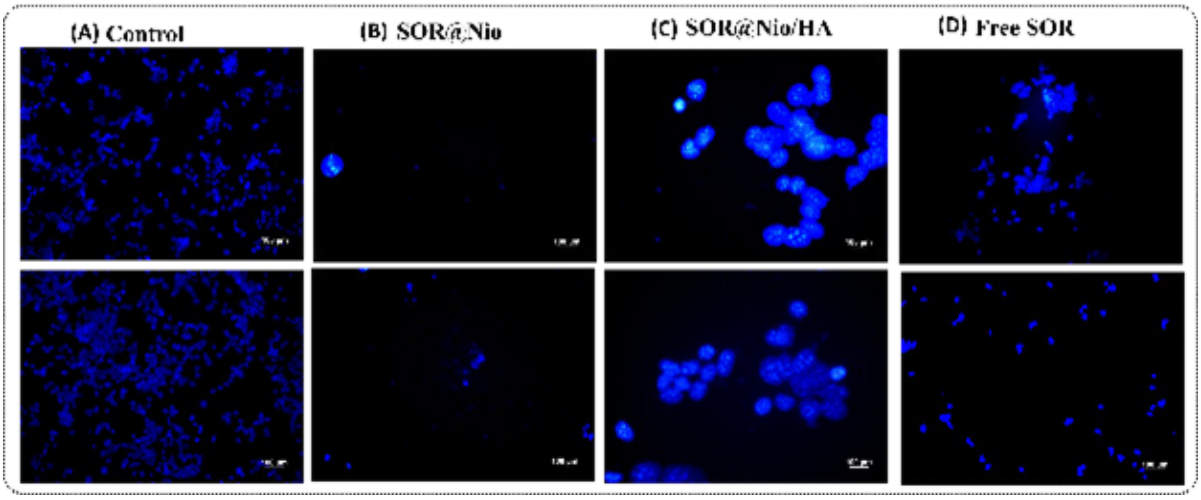

Figure 11. 4′,6-diamidino-2-phenylindole (DAPI) fluorescence (blue) of CAL27 nuclei after 24 hr under the indicated treatments
Representative fields show nuclear condensation/fragmentation in apoptotic groups versus dense, uniform nuclei in viable groups; scale bar=100 µm

experiments. In drug loading analysis, mechanistically, moderate cholesterol maintains sufficient membrane rigidity to limit back-diffusion while avoiding excessive stiffening that would reduce bilayer accommodation of hydrophobic sorafenib-consistent with the significant A×B interaction found in the response-surface analysis. As mentioned before, for the optimized formulation, DL=7.2±0.4 % (w/w), corresponding to 0.072±0.004 mg sorafenib per mg vesicle (total surfactant+cholesterol+drug solids). Notably, HA grafting did not significantly change the EE relative to that of non-coated niosomes (P>0.05), consistent with coupling occurring predominantly at the corona without disrupting the bilayer core. However, prolonged storage at 25 ˚C caused a gradual decrease in EE (e.g., -12% at day 60), whereas storage at 4 ˚C maintained ≥ 90 % of the initial EE, matching the PDI trends and suggesting fusion-assisted leakage at higher temperatures.

In FT-IR Section, the characteristic peaks of sorafenib, hyaluronic acid, and niosomes were present in the SOR@Nio/HA spectrum, suggesting that the formulation retained the molecular integrity of the drug while incorporating the stabilizing hyaluronic acid layer. These interactions indicate a well-constructed delivery system with the potential for targeted delivery to OSCC cells via the CD44 receptor. As it can be observed in the TGA results, the thermal signatures align with zeta-potential inversion and FTIR amide I/II growth; the absence of a SOR melting peak supports amorphization/encapsulation. Practically, storage at 4 ˚C is recommended (prolonged 25 ˚C can increase PDI and reduce EE). In the stability analysis result it can be seen that the HA corona increases the hydrated interfacial layer; at 25 °C greater HA chain mobility and higher bilayer fluidity lower interfacial modulus, promoting mild intervesicular bridging/aggregation (size/PDI increased) and slightly higher membrane permeability (EE decreased). Thus, 4 ˚C storage is preferred to preserve colloidal integrity and drug retention.

Regarding the mechanism of drug release, protonation of HA carboxylates and increased bilayer fluidity at low pH elevate permeability, while a deprotonated HA corona at neutral pH forms a gel-like barrier that slows diffusion. Functionally, this affords low leakage in circulation (<1% h^{-1} at 7.4, 24 hr) and rapid post-endocytic release at endolysosomal pH, yielding an on/off ratio of 3-4; performance surpasses plain sorafenib niosomes that released 61% in 4 hr irrespective of pH.

The enhanced cytotoxicity of the final formulation can be attributed to better cellular uptake of niosome-encapsulated sorafenib and more efficient intracellular delivery. The active targeting by HA likely contributed, as HA-coated niosomes can bind CD44 receptors on CAL27 cells and undergo endocytosis, concentrating the drug inside cancer cells. In contrast, free sorafenib enters the cells mainly via passive diffusion, which may be less efficient and can be affected by drug efflux pumps. These results underscore a key therapeutic advantage of HA-coated sorafenib-loaded nanoniosomes in the context of OSCC, representing an improved therapeutic index, whereby enhanced cytotoxicity is exerted on OSCC cells with minimal adverse effects on non-cancerous cells. Notably, blank Nio/HA exhibited no significant cytotoxicity, confirming the biocompatibility of the carrier system and excluding non-specific toxicity owing to the nanocarrier itself. Comparable findings have been reported for other HA-targeted nano-delivery systems. Similarly, Fathalizadeh *et al.* reported that HA-functionalized α-terpineol-loaded niosomes lowered the IC_{50} in PANC-1 cancer cells from >500 µg/ml to 237 µg/ml; blank niosomes showed 100% viability at 250 µg/ml and became significantly cytotoxic only at 500 µg/ml (18).

In the inflammatory mediators evaluation it can be observed that the data indicate transcriptional modulation of NF-κB–related targets with a pro-apoptotic shift; direct pathway activity readouts (nuclear p65, IκBα phosphorylation/degradation, κB-luciferase) and protein-level confirmation (COX-2/MMP-9) were not included and are suggested for future work. Also, it can be seen from flowcytometry assay that notably, HA-Nio-SOR shifted the distribution toward early apoptosis (Q3/Q2=3.1 vs 2.6 for free SOR), consistent with a more regulated apoptotic program and improved intracellular delivery; CD44 mediation was not directly tested here. Although total apoptosis with HA-Nio-SOR was lower than free SOR, the shift toward early apoptosis (Q3/Q2=3.1) with <2% necrosis indicates better preservation of membrane integrity and a more controlled death program. This phenotype aligns with the pH-triggered endolysosomal release and down-regulation of COX-2/MMP-9, suggesting efficient intracellular exposure with reduced pro-inflammatory spillover; confirmation with protein-level NF-κB assays and receptor-blocking studies is warranted.

Finally, the optical DAPI readout sensitively captures chromatin condensation/fragmentation, consistent with our Annexin V/PI data and the pro-apoptotic increased BAX/decreased BCL-2 pattern. The HA corona likely improves intracellular exposure via CD44-mediated uptake and, together with pH-triggered endolysosomal release, biases death toward an ordered (early-apoptotic) program with minimal necrosis. Further receptor-blocking/protein-level assays would solidify this mechanism. In general, sorafenib strategies in OSCC/HNSCC: NF-κB evidence and gaps are represented in Table 5.

Conclusion

In this study, hyaluronic-acid–coated niosomes encapsulating sorafenib (SOR@Nio/HA) were developed to exploit CD44-mediated uptake and thereby enhance pharmacological suppression of NF-κB signaling in OSCC. The nanoformulation exhibited a hydrodynamic diameter of 177±8 nm (PDI=0.23-0.26) and high encapsulation efficiency (86.34%), with pH-responsive release favoring endo/lysosomal conditions (45% at pH 5.5 vs 30% at pH 7.4, 24 hr). In CAL27 cells, SOR@Nio/HA increased cytotoxic potency relative to free sorafenib, lowering the IC_{50} from 11.8±1.1 µM to 5.2±0.9 µM (P<0.01), and promoted apoptosis as confirmed by Annexin V/PI staining. At the transcriptional level, canonical NF-κB targets were down-regulated (COX-2 to 0.35-fold and MMP-9 to 0.32-fold of control), accompanied by a pro-apoptotic shift in the BAX/BCL-2 axis, consistent with on-target inhibition of inflammatory and invasive programs. These findings indicate that HA decoration and niosomal encapsulation jointly improve intracellular delivery and mechanistic efficacy of sorafenib through CD44-facilitated internalization and NF-κB pathway repression. Given the nanoscale size and pH-triggered release profile, the platform is well positioned for tumor-selective delivery, while potentially mitigating

Table 5. Sorafenib strategies in OSCC/HNSCC: NF-κB evidence and gaps

Study Reference (Author, Year)	Nano-/Delivery Platform (Size)	Active-Ligand	OSCC/HNSCC Model	Principal Anti-Tumor Findings	NF-κB Pathway Data	Apoptosis Readouts	Key Caveats / Knowledge Gaps
Lim *et al*., 2023 (19)	Solid self-nanoemulsifying drug delivery system (SNEDDS; <80 nm)	None	KB cells (human oral carcinoma)	Enhanced aqueous solubility and dissolution; SNEDDS reduced cell viability more than free sorafenib ($p < 0.01$)	Not reported	Annexin V staining indicated earlier apoptotic shift compared to free drug	*In vitro* only; NF-κB not examined; no *in vivo* biodistribution
Poojari *et al*., 2016 (20)	$CaCO_3$ core, layer-by-layer polyelectrolyte sorafenib nanoparticles (100-300 nm)	None	KB cells	LbL-NP reduced proliferation and migration; IC_{50} approximately halved compared to free sorafenib; endosomal uptake visualized by CLSM	Not reported	Flow cytometry showed total apoptosis greater than free sorafenib at matched dose	No animal studies; NF-κB axis untested; lacks active-targeting
Hsu *et al*., 2014 (3)	Free sorafenib combined with ionizing radiation (*in vitro* radiosensitization)	None	SAS & SAS/NF-κB-luc2 cells	Combination killed over 80% of cells and synergistically suppressed clonogenic survival	Luciferase assay, EMSA, and Western blots showed radiation-induced NF-κB activity decreased by approximately 70%; COX-2, *MMP-9*, XIAP down-regulated	Increased cleaved *caspase-3/8*; mitochondrial and death-receptor pathways activated	Not a nanoformulation; requires pharmacokinetic optimization
Hsu *et al*., 2015 (2)	Free sorafenib combined with radiation (orthotopic xenograft)	None	SAS/luc tongue-tumor model (nude mice)	Tumor volume reduced by 67%; bone invasion prevented; micro-CT showed minimal mandibular damage	NF-κB DNA-binding and p65 IHC strongly suppressed; downstream VEGF, COX-2, *MMP-9* all decreased	Immunoblots indicated increased cleaved *caspase-3/8*, cytochrome c	Systemic sorafenib dosing; no drug carrier; potential off-target toxicities
Yadav *et al*., 2011 (21)	Free sorafenib combined with cisplatin/5-FU and radiation (chemoradiosensitizer)	None	UM-SCC-74A & CAL27 xenografts	Combination therapy shrank tumors by approximately 60% compared to control and doubled microvessel apoptosis	NF-κB not measured; mechanistic focus on ERCC-1/XRCC-1 down-regulation	TUNEL assay and cleaved PARP signal increased with triple combination	Lacks nanoparticle carrier; NF-κB inference indirect; limited OSCC cell line diversity
Elser *et al*., 2007 (22)	Free sorafenib (oral administration)	None	Phase II trial in recurrent/metastatic HNSCC patients	Modest clinical activity; partial response rate of 2%; median progression-free survival of 1.8 months	NF-κB pathway not assessed	Not reported	No biomarker stratification; limited efficacy as monotherapy
He *et al*., 2022 (23)	PDX model	None	OSCC PDX models	Established and validated PDX models that recapitulate the complex oral microenvironment	Not applicable	Not applicable	Provides a platform for future evaluation of sorafenib-based therapies

systemic exposure. Limitations include reliance on a single OSCC line and *in vitro* readouts. Future work should establish in-vivo biodistribution, pharmacokinetics, and safety, quantify CD44-dependent uptake across heterogeneous OSCC models, and assess antitumor efficacy and stromal/immune modulation in orthotopic systems. Overall, SOR@Nio/HA emerges as a targeted nanotherapeutic candidate that warrants translational evaluation for OSCC.

Acknowledgment

Nothing to declare.

Funding

This study did not receive any funding.

Authors' Contributions

T W, B G, and Y L conceived the study and contributed to visualization, investigation, writing the original draft, and funding acquisition. Z W and Y L performed formal analysis and investigation. T W and Z W helped with investigation and methodology. B G and Y L contributed by formal analysis and resource acquisition. Y L and Z W contributed by conceptualization, resource acquisition, and supervising.

Conflicts of Interest

The authors declare no competing interests.

Declaration

We acknowledge the use of Grammarly and PaperPal to check grammar and language editing. Subsequently, the entire manuscript was thoroughly read, revised, checked, and approved by all authors.

References

1. Niklander SE. Inflammatory mediators in oral cancer: Pathogenic mechanisms and diagnostic potential. Front Oral Health 2021; 2: 642238.
2. Hsu F-T, Chang B, Chen JC-H, Chiang IT, Liu Y-C, Kwang W-K, *et al*. Synergistic effect of sorafenib and radiation on human oral

carcinoma *in vivo*. Sci Rep 2015; 5: 15391.
3. Hsu FT, Chang B, Chiang IT, Wu TH, Hwang JJ. Synergistic effect of sorafenib with ionizing radiation on human oral cancer cells. In vivo 2014; 28: 925-933.
4. Raeisi Estabragh MA, Behnam B, Torkzadeh-Mahani M, Pardakhty A. Niosome as a drug delivery carrier for sorafenib: Preparation, investigation of physicochemical properties, and *in vitro* effects on HepG2 cell line. Adv Pharm Bull 2024; 14: 836-845.
5. Mesrati MH, Tajudin AA, Masarudin MJ, Alamassi MN, Abuhamad AY, Syahir A. Hyaluronic acid/chitosan-coated poly (lactic-co-glycolic acid) nanoparticles to deliver single and co-loaded paclitaxel and temozolomide for CD44+oral cancer cells. OpenNano 2023; 12: 100166.
6. Mirhashemi M, Sadeghi M, Ghazi N, Saghravanian N, Dehghani M, Aminian A. Prognostic value of CD44 expression in oral squamous cell carcinoma: A meta-analysis. Ann Diagn Pathol 2023; 67: 152213.
7. Hepkema WM, Horbach S, Hoek JM, Halffman W. Misidentified biomedical resources: Journal guidelines are not a quick fix. Int J Cancer 2022; 150: 1233-1243.
8. Bray F, Laversanne M, Sung H, Ferlay J, Siegel RL, Soerjomataram I, *et al*. Global cancer statistics 2022: GLOBOCAN estimates of incidence and mortality worldwide for 36 cancers in 185 countries. CA Cancer J Clin 2024; 74: 229-263.
9. Dehghan S, Naghipour A, Anbaji FZ, Golshanrad P, Mirazi H, Adelnia H, *et al*. Enhanced *in vitro* and *in vivo* anticancer activity through the development of Sunitinib-Loaded nanoniosomes with controlled release and improved uptake. Int J Pharm 2023; 640: 122977.
10. Lih E, Choi SG, Ahn DJ, Joung YK, Han DK. Optimal conjugation of catechol group onto hyaluronic acid in coronary stent substrate coating for the prevention of restenosis. J Tissue Eng 2016; 7: 2041731416683745.
11. Mosmann T. Rapid colorimetric assay for cellular growth and survival: Application to proliferation and cytotoxicity assays. J Immunol Methods 1983; 65: 55-63.
12. Danaei M, Dehghankhold M, Ataei S, Hasanzadeh Davarani F, Javanmard R, Dokhani A, *et al*. Impact of particle size and polydispersity index on the clinical applications of lipidic nanocarrier systems. Pharmaceutics 2018; 10: 57.
13. Dang Y, Guan J. Nanoparticle-based drug delivery systems for cancer therapy. Smart Mater Med 2020; 1: 10-19.
14. Zhang W, Xu W, Lan Y, He X, Liu K, Liang Y. Antitumor effect of hyaluronic-acid-modified chitosan nanoparticles loaded with siRNA for targeted therapy for non-small cell lung cancer. Int J Nanomed 2019; 14: 5287-5301.
15. Moammeri A, Abbaspour K, Zafarian A, Jamshidifar E, Motasadizadeh H, Dabbagh Moghaddam F, *et al*. pH-responsive, adorned nanoniosomes for codelivery of cisplatin and epirubicin: Synergistic treatment of breast cancer. ACS Appl Bio Mater 2022; 5: 675–690.
16. Bian Y, Guo D. Targeted therapy for hepatocellular carcinoma: Co-delivery of sorafenib and curcumin using lactosylated pH-responsive nanoparticles. Drug Des Devel Ther 2020; 14: 647-659.
17. Saharkhiz S, Zarepour A, Zarrabi A. A new theranostic pH-responsive niosome formulation for doxorubicin delivery and bio-imaging against breast cancer. Int J Pharm 2023; 637: 122845.
18. Fathalizadeh M, Tabrizi MH, Tehranipour M. A novel alpha-terpineol-loaded niosome formulation coated with hyaluronic acid and evaluation of its anticancer properties *in vitro*. J Mol Liq 2025; 424: 127139.
19. Lim C, Lee D, Kim M, Lee S, Shin Y, Ramsey JD, *et al*. Development of a sorafenib-loaded solid self-nanoemulsifying drug delivery system: Formulation optimization and characterization of enhanced properties. J Drug Deliv Sci Technol 2023; 82: 104374.
20. Poojari R, Kini S, Srivastava R, Panda D. Intracellular interactions of electrostatically mediated layer-by-layer assembled polyelectrolytes based sorafenib nanoparticles in oral cancer cells. Colloid Surf B Biointerfaces 2016; 143: 131-138.
21. Yadav A, Kumar B, Teknos TN, Kumar P. Sorafenib enhances the antitumor effects of chemoradiation treatment by down-regulating ERCC-1 and XRCC-1 DNA repair proteins. Mol Cancer Ther 2011; 10: 1241-1251.
22. Elser C, Siu LL, Winquist E, Agulnik M, Pond GR, Chin SF, *et al*. Phase II trial of sorafenib in patients with recurrent or metastatic squamous cell carcinoma of the head and neck or nasopharyngeal carcinoma. J Clin Oncol 2007; 25: 3766-3773.
23. He F, Zhou X, Huang G, Jiang Q, Wan L, Qiu J. Establishment and identification of patient-derived xenograft model for oral squamous cell carcinoma. J Oncol 2022; 2022: 3135470.